GEOFIZIKA VOL. 43 2026

DOI: https://dx.doi.org/10.15233/gfz.2026.43.4
Professional paper

Geotechnical parameters evaluation using Multichannel Analysis Surface Waves (MASW) in the upstream basin of Chaq-Chaq Dam in Sulaimani, NE Iraq

Sazan S. Mohammed[1], Abdulla K. Amin[2] and Ezzadin N. Baban[3]*

[1] Governorate of Sulaimani, Main Qliasan street, 46001, Sulaimani, Kurdistan Region, Iraq

[2] Department of social sciences, College of basic education, University of Sulaimani, Tasluja Street 1 Zone 501, 46001, Sulaimani, Kurdistan Region, Iraq

[3] Department of Geology, College of Science, University of Sulaimani, Tasluja Street 1 Zone 501, 46001, Sulaimani, Kurdistan Region, Iraq

Received 21 May 2025, in final form 22 October 2025

The velocities of the compressional and shear waves (V_P and V_S) were determined for seven parallel Multichannel Analysis of Surface Waves (MASW) traverses within the upstream basin of Chaq-Chaq Dam in Sulaimani, Kurdistan Region- Iraq. These traverses were executed with a spacing of 2 meters (m) between the geophones. The objective of this study was to investigate subsurface geological features, determine the depth to bedrock, assess bedrock strength, calculate primary and shear wave velocities, and explore potential causes for the collapse of the constructed Chaq-Chaq Dam. Data was collected using Geometrics Seismodule Controller software and processed using ParkSeis Software. The velocity results indicate that the study area comprises three geological layers: a surface soil layer on top, a middle layer of rock fragments, and a limestone layer at the bottom. The calculated Poisson's ratio based on V_P and V_S values for these three layers ranges between 0.35 and 0.39 for the first layer, 0.30 and 0.33 for the second layer, and 0.24 and 0.25 for the third layer. These results suggest that the first layer has relatively high values of Poisson's ratio, indicating an incompetent soil layer. The second layer exhibits moderate values, suggesting a fairly competent layer of rock fragments, while the third layer has low values, indicating a well-competent limestone layer. The findings also highlight deficiencies in the dam's design, particularly in the southern parts where most of the traverses show the presence of sinkholes. These sinkholes are likely caused by water infiltration during the rainy winter season. When water pressure is applied to the dam, these sinkholes in the southwestern portion could be attributed as the cause of the dam collapsing. Additionally, the dam side was not properly intertied with the rocks forming the right bank of the dam.

Keywords: MASW, dynamic moduli, shear wave velocity, Chaq-Chaq dam, Iraqi Kurdistan

1. Introduction

Dams offer numerous advantages, including water storage for irrigation purposes and flood prevention by collecting and releasing excess water as needed. One of the most useful geophysical techniques is known as shallow seismic refraction, which can be used to identify the depth of the bedrock, and geotechnical parameters of the investigated sites (Meneisy et al., 2023).

Dam failures happen throughout the world. According to the reports International Commission on Large Dams (ICOLD,1998), about 38% of dam failures were caused by over topping related to the inadequate spillway capacity. Also, about 33% of dam failures were related to seepage or piping. Even if the reason may vary, almost all dam failures begin with a breach formation. Zhang et al. (2009) applied multi-parameter nonlinear regression analysis and found out that dam erodibility is the most important factor, influencing the other breaching parameters and that the equations for predicting the breach geometric parameters appear to be more accurate, than those for predicting the peak outflow rate and the failure time (Xiong, 2011). A breach is defined as an opening formed in the dam body and its gradual expansion results in the destructive propagation of the large volume of water in the reservoir to the downstream (Wahl, 1998). Breach geometry (e.g., breach depth, width, and breach side slope factor), timing (initial breach time, Breach Formation Time (BFT), etc.), failure mode, and breach progression need to be estimated precisely in dam failure modeling (Froehlich, 2008). Baban et al. (2022) applied the seismic refraction tomography method for the first time to assess the failure of the Chaqchaq Dam in NW Sulaimani city, Kurdistan Region, Iraq. Their findings suggest that the fundamental design of the Chaqchaq Dam construction lacked scientific principles, and the presence of sinkholes may be a contributing factor to the dam's collapse.

The choice of geophysical methods depends on the target and geological conditions encountered in the field (Tsai and Lin, 2022). According to Park and Carnevale (2009), conventional 2D Multichannel Analysis of Surface Waves (MASW) investigations focus on the inline propagation of planar surface waves, providing a 2D shear velocity (V_S) map that represents the cross-sectional image of subsurface stiffness distribution with minimal influence from offline features like side scattering. Karray et al. (2010) state that MASW has gained acceptance in the geophysics community, primarily for understanding material compaction and variations in lithological layer thickness. To enhance dispersion image resolution at lower frequencies, Taipodia et al. (2018) recommend using a heavier source or adopting multiple stacking of dispersion images generated from low-energy impacts. Arisona et al. (2017) utilized MASW to evaluate the boundary and depth of soil structure for geotechnical site investigation in Pedas, Negeri Sembilan, Peninsular Malaysia. Ashraf et al. (2018) demonstrated that MASW, as a geophysical method, can classify sites in both soft and hard ground. Abudeif et al. (2019) applied 2D MASW in New Akhmim city, Sohag, Upper Egypt, for geotechnical engineering soil evaluation. Shear wave velocity is a critical param-

eter for earthquake geotechnical engineering. Netto et al. (2020) emphasized that geophysical surveys in dam structures aim to detect internal fluid flow, identify voids or craters, locate possible fracture zones, and determine variations in massif saturation levels characteristics directly linked to dam stability. Rahnema et al. (2021) used surface waves (R-wave) and seismic refraction (P-wave) methods to detect cavities and intrusions of different sizes and depths.

Duan et al. (2024) were concluded that the primary cause of the dam failure of the model dam was the rise in water level. The foundation of the dam became liquefied due to the rise in water level. The liquefaction of tailing at the base of the dam resulted in slip flow, which led to the instability of the dam's upper body. Then, the tailing in the middle part lost the support of the dam foot, which lay the foundation for the crack on the dam surface after the overflow. When the water in the pond exceeded the height of the dam, it would typically follow the fractures or slide down the gullies formed by the liquefaction of the dam's foundation. The presence of the scarp significantly amplified the erosive impact of water flow, leading to the rapid destruction of the dam through erosion.

2. Location and topography of the area studied

The studied area includes both the Chaq-Chaq Dam and its upstream (reservoir) section, situated approximately 2 km northwest of Sulaimani city in the Kurdistan Region of Northeast Iraq. The area lies between the western and eastern sides of the dam, influenced by a strike-slip fault that cuts through the Sulaimani anticline structure. The predominant geological formation in this region is the Kometan Formation, primarily composed of limestone (Al-Hakari, 2011).

Geographically, the area falls within zone 38S of the UTM coordinate system, specifically between coordinates 3940267N–3940208N and 534696E–534830E. Additionally, it extends from 3939971N–3940036N and 534783E–534650E. The study area, which encompasses the reservoir basin, covers approximately 45,039 m^2 as shown in Fig. 1. Minimum elevation of the study area lies at southwest part near west side of Chaq-Chaq dam and the higher area located at the eastern part of the area ranges between 768-771m (Baban et al., 2022).

3. Geology and tectonic setting

The Zagros orogenic belt resulted from the collision of the Arabian and Eurasian Plates during the Cenozoic era up to the present day (Alavi, 2004; Alavi, 2007), as depicted in Fig. 2. The Iraqi territory serves as the northeastern extension of the Arabian Platform, which surrounds the Arabian Shield. Early researchers divided the Arabian Platform within Iraq into two major parts: a stable region to the southwest and an unstable region to the northeast (Dunnington, 1958). Over time, subsequent researchers adapted and refined these

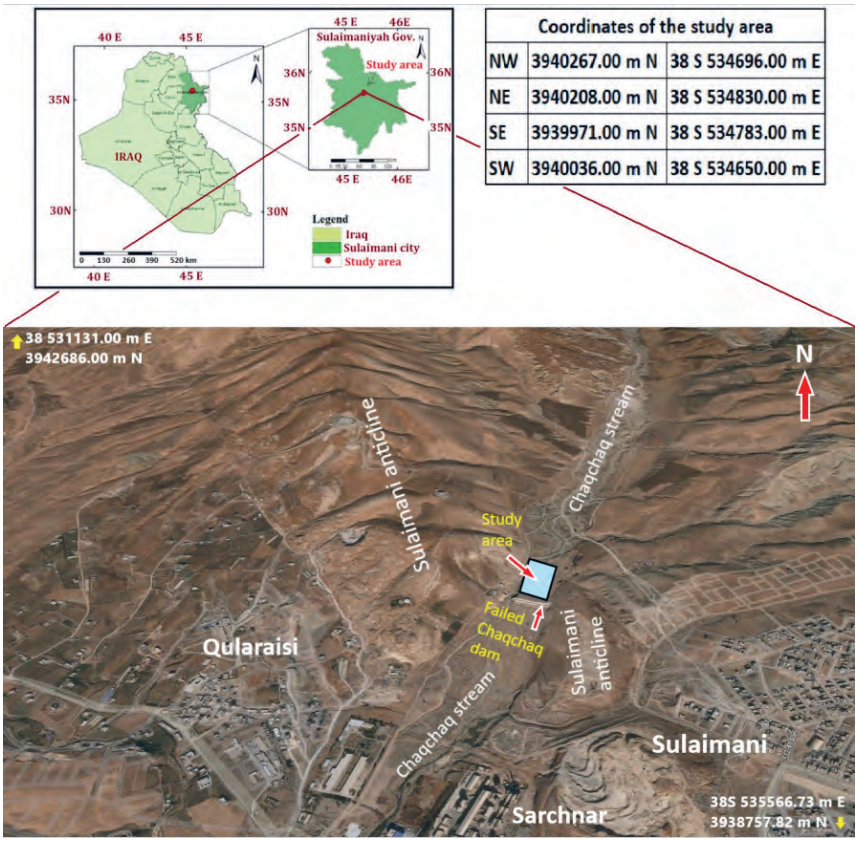


Figure 1. Location map of the study area (Baban et al., 2022).

definitions, further subdividing the area into smaller zones and subzones to describe Iraq's structural framework (Ditmar, 1971; Buday, 1980).

Tectonically, Iraq can be categorized into two main tectonic units: the Alpine Geosyncline and the Nubian-Arabian Platform. The structure and development of Iraq are significantly influenced by its position at the boundary between these two major Phanerozoic tectonic units in the Middle East (Buday and Jassim, 1987). Buday (1980) and later Buday and Jassim (1987) further divided the Iraqi territory into a Stable Shelf (located in the southwest) and an Unstable Shelf (situated in the northeast). The Unstable Shelf was then subdivided into Mesopotamian, Foothill, High Folded, and Geosyncline Zones.

The lithology and stratigraphic succession in the study area primarily consists of the Kometan Formation, which was initially described by Jassim and Goff (2006). Lithologically, this formation comprises white-to-light-gray, hard, uniform, and medium-bedded limestone, as well as chalky limestone (Al-Qayim et al., 2012). The Kometan Formation is exposed in the northern, northeastern,

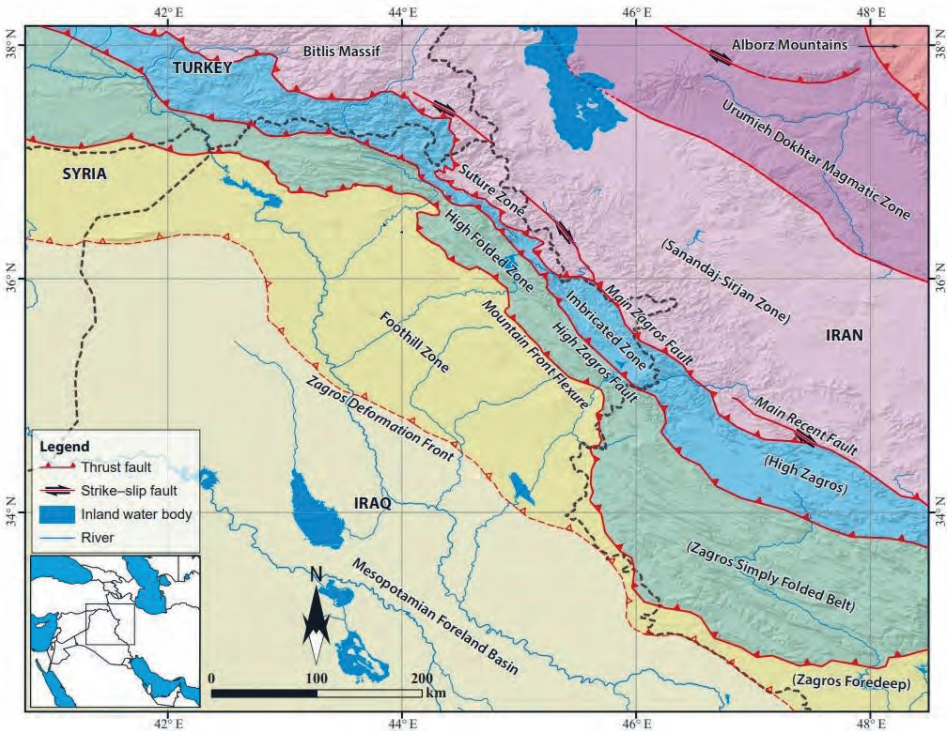


Figure 2. Tectonic subdivision of the NW segment of the Zagros Fold–Thrust Belt (modified by Zebari, et al., 2019)

and northwestern parts, including the limbs of the Azmar-Goizha and the Plunge of Piramagrun. It also occurs in the Sulaimani anticlines and the western portion of Sulaymaniyah city, which encompasses our study area. Additionally, field observations reveal Quaternary sediments, including two units of alluvium and some residual slope wash soil layers exposed in the Chaq-Chaq valley terraces. These sediments belong to different periods of recent time.

The total length of each traverse varied: MS-Tr-1 covered 170 m, MS-Tr-2 was 92 m long, and MS-Tr-3 spanned 160 m. For all other traverses, the total length was 230 m. P-waves were generated using the 10 LB sledgehammer as the energy source, with a record length set at 1 second and a sample interval of 0.500 ms (see Table 2).

4. MASW data acquisition and interpretation

4.1 Data acquisition

MASW fieldwork is the most important technique of the seismic survey. It must be performed with safe and a high accuracy, any mistakes in fieldwork

measurements will reflect on the other phases of the survey. A reconnaissance survey was carried out by the researchers before conducting a field work, through visiting the surrounding Qularaisi and Chaq-Chaq area in order to get a significant imagination about the surface geology and topography of the areas to decide which area is more suitable for the research paper. The Qularaisi area, characterized by undulating and gentle slope topography especially near the cliff of the foot hill of Piramagrun continuation is suitable for constructing small dam or ponds, whereas the previously failed dam, situated on the plunge of the Sulaimani anticline, benefits from the presence of the Kometan Formation on both sides, providing a solid foundation for the dam's shoulder. This alignment with the study's objectives and previous seismic refraction tomography method study according to Baban et al. (2022) involves applying the Multichannel Analysis of Surface Waves (MASW) technique to calculate seismic velocities, thicknesses, depths, and dynamic moduli of elasticity across different layers, all aimed at achieving the primary research goals.

Fieldwork was meticulously planned by dividing the study area into seven MASW traverses: MS-Tr-1, MS-Tr-2, MS-Tr-3, MS-Tr-4, MS-Tr-5, MS- Tr-6, and MS-Tr-7 as shown in Table 1.

These traverses trend from southwest (SW) to northeast (NE), each of them parallel to each other (as depicted in Fig. 3). Outcrops of the Kometan Formation are visible in the field. This formation primarily consists of limestone and can be observed on both the east and west sides of the study area (as depicted in Fig. 4), shaping the valley basin within the research area (the dam basin). Recent deposits, including soil and rock fragments, contribute to the variability in soil layer thickness across different locations, with certain areas exhibiting a thickness of less than 1 m.

The most accurate method for assessing geotechnical parameters, particularly dynamic moduli of elasticity, is the MASW (Multichannel Analysis of Surface Waves) technique. MASW is highly effective for measuring shear velocity

Table 1. Number of traverses, direction, and coordinates for MASW method.

No. of traverses	South coordinates		North coordinates	
	East	North	East	North
MS-Tr-1	534783	3939971	534830	3940208
MS-Tr-2	534766	3939981	534811	3940216
MS-Tr-3	534746	3939992	534783	3939971
MS-Tr-4	534729	3939998	534776	3940231
MS-Tr-5	534712	3940008	534758	3940240
MS-Tr-6	534694	3940014	534739	3940247
MS-Tr-7	534650	3940036	534696	3940267



Figure 3. Locations of MASW traverses (Google Earth, https://earth.google.com).

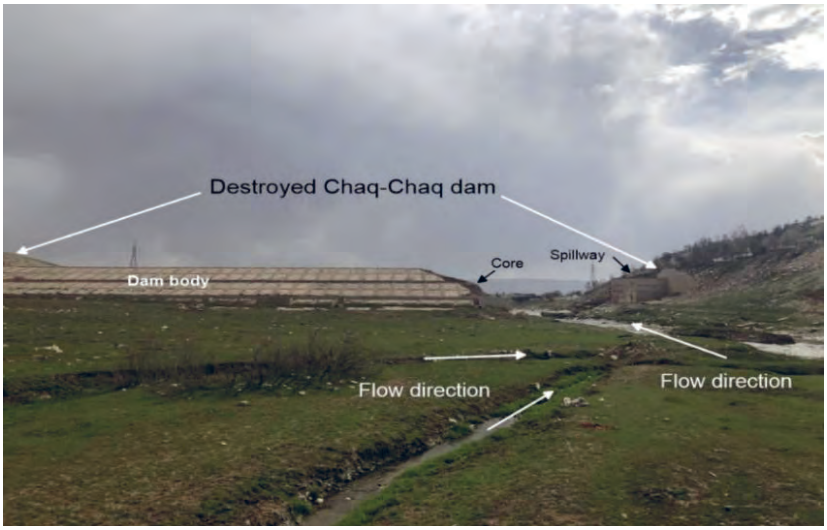


Figure 4. Photograph of Chaq-Chaq valley and failed dam.

(V_S), which plays a crucial role in calculating various elastic moduli, including Poisson's ratio, Young's modulus, shear modulus, bulk modulus, and compressibility. These parameters are essential for identifying geological features, determining bedrock locations, detecting voids, evaluating collapse potential, and identifying fractures.



Figure 5. Geophones configuration with 2 m spacing.

During the survey, a 10 LB sledgehammer served as the energy source. The initial step involved striking along a straight line to ensure precise placement of stakes at regular intervals. In the MASW method, geophone spacing was set at 2 m (as shown in Fig. 5). Traverses were spaced 20 m apart, except for the last traverse, which had a spacing of 50 m.

The first geophone (offset) was positioned 5 m away from the shot location. This method involved shifting one geophone from the start of the traverse toward

Table 2. Acquisition parameters of seismic refraction traverses for MASW technique.

Data formatting	SEG
Geometry	Linear Spread
Number of receivers	24
Receiver spacing	2 m
Receiver type	Vertical geophone 14 Hz
Shot spacing	5 m
Source type	Sledgehammer (10 LB)
Number of stackings	5
Sampling interval	0.500 ms
Record length	1 Second
Spread Cable	24 Takeout at 5m interval
Trigger extension cable	300 FT (92 m)
Aluminum strike plate	6" x 6" x 1"
Battery	12V, 60Ah

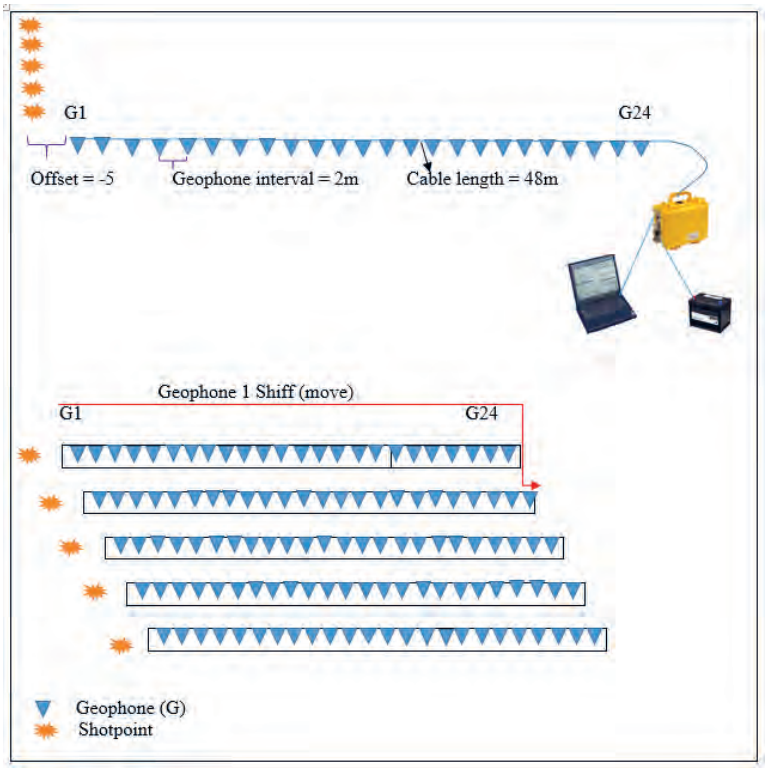


Figure 6. MASW data acquisition layout, first geophone shifted to the end.

the end. The process was repeated until reaching the total length of 230 m for the traverse. Fig. 6 displays the MASW layout. A total of 94 shots (data points) were recorded for the 230 m length. MASW was used to generate and record S-waves, captured using five stacks of vertical geophones and repeated strikes (shots) on a metal striker plate. Vertical stacking of multiple strikes (shots) is a data acquisition technique used to reduce ambient noise, and improve the signal-to-noise ratio (S/N), which is particularly beneficial in urban areas where this survey was conducted.

4.2. Data processing

Rayleigh-type seismic surface wave surveys are processed using ParkSeis (PS) software (Park, 2015). PS analyzes the fundamental-mode (M0) dispersion curve of Rayleigh waves to create shear-wave velocity (V_S) profiles (1-D or 2-D). The data for multichannel analysis surface wave (MASW) is recorded by a 24-channel Geode seismograph. To preserve the field records, the Society of Exploration Geophysicist SEG-2 format is used to import multiple seismic files

from the first traverse into PS software. For this purpose, the source/receiver setup from the main menu applied to encode the correct distance and location information for each seismic channel, including source and receiver distances along the survey traverse, spacing between geophones, source offset, and movement (shifting) of the source and receiver which is crucial for accurate MASW analysis and to produce a correct S-wave velocity (V_S) profiles (Park, 2021). Then save input records as a single file ('PS' format) and ready for the regular MASW data analysis using a conversion module ('TXT2PS') found in the main menu's 'Utility' section. The output file saved from this step will therefore have as many of such images as number of seismic records in the input file.

The quality and size of the generated dispersion image depend on several parameters including data acquisition and pre-processing steps, which collectively influence the resolution of the energy distribution in the frequency-phase velocity domain. Seismic wave characteristics are analyzed using dispersion curves, which are automatically generated from dispersion images although need to be manually edited to fix processing errors. The manual editing may be necessary to adjust the extracted dispersion curve by adding, deleting, or moving points in order to accurately record the direction of the wave, whereas the automatic method detects the dominant wave energy in dispersion images. Mispicks in the MASW method, which can lead to incorrect S-wave velocity (V_S) profiles, are identified by comparing the extracted dispersion curves to expected proper-

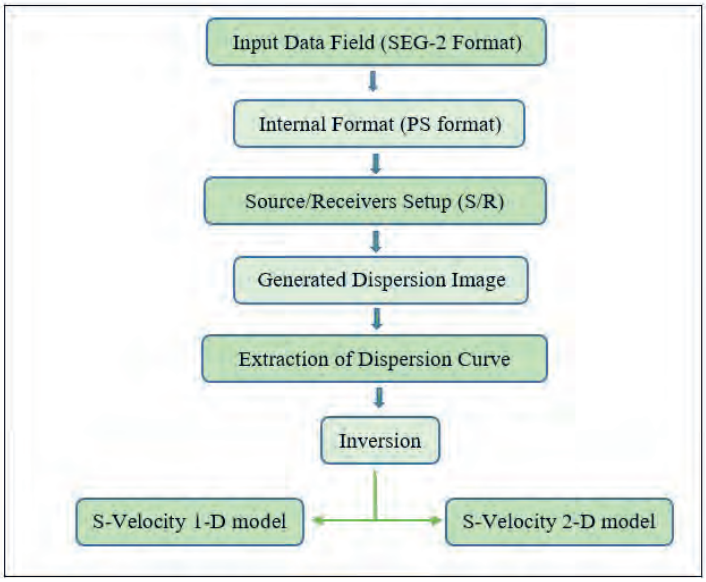


Figure 7. Flow chart shows data processing for MASW by ParkSeis Software (modified after Park, 2015).

ties, such as a continuous increase in velocity with depth, compared to previous study, and by identifying unusual or "anomalous" curves. In this study range for the fundamental mode applications is 20-50 Hz (minimum frequency is 20 and maximum frequency is 50).

Finally, clicking the inversion button generates (1-D or 2-D) from input dispersion curve(s). The main inversion parameters related to dispersion imaging processing, which is basically a wave field transformation operation that converts seismic wave fields in offset-time (x-t) domain into those in phase velocity-frequency (Pv-f) domain.

The flowchart in Fig. 7 illustrates all the processing steps applied to the MASW field data traverses.

4.3. Interpretation of MASW

The 2D shear wave velocity traverses were derived from the northern part of the dam reservoir using the MASW technique by PS Software. Bedrock is exposed at shallow depths. Firstly, the source/receiver setup was completed as shown in Fig. 8, with geometry systematically adjusted based on using numbers to identify the numerically renamed data. The seismic refraction configurations for these records are linearly interpolated in surface coordinates for both source and receivers. The resultant seismic refraction configuration for all 94 records in an input seismic data is displayed below with distance surface coordinates. Corrected original seismic refraction data setup is considered as imported files saved as a single SR-coded file ["SeismicData(SR).dat"] (Park, 2015).

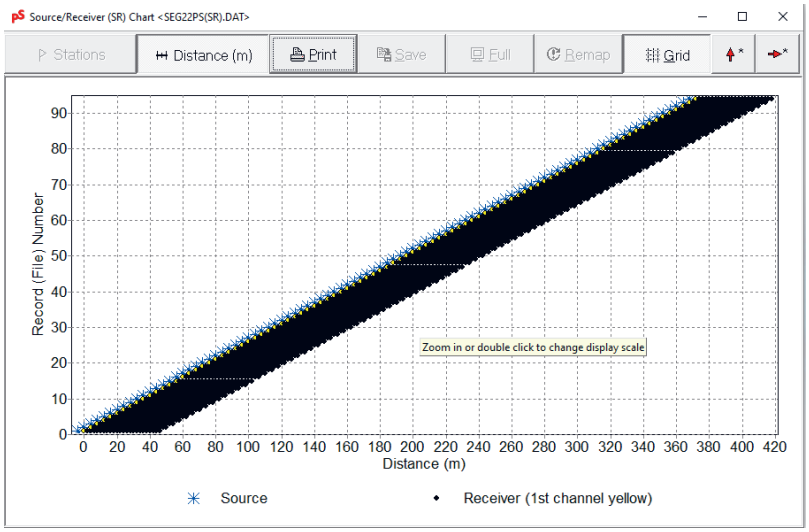


Figure 8. Illustration of the source/receiver setup for the Tr-7 traverse.

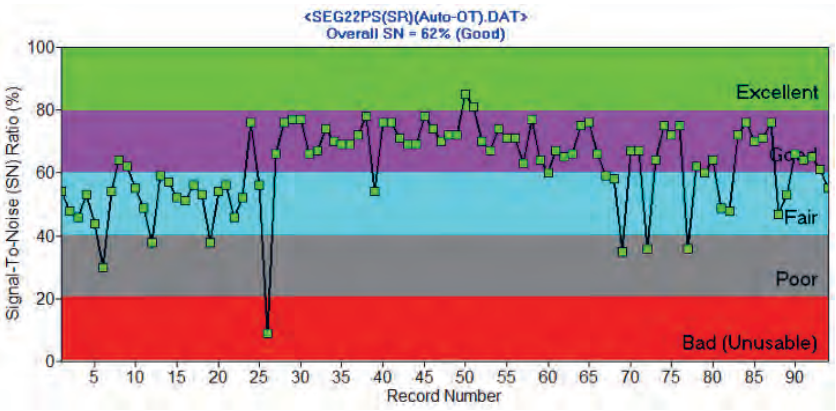


Figure 9. Signal-to-noise ratio for all data in the Tr-7 traverse.

Afterward, all data for each traverse underwent signal-to-noise (SN) ratio evaluation by scanning seismic data automatically, as shown in Fig. 9. In this section an automatic process is used to evaluate the SN ratio of each record in the seismic data file [*(SR)*.dat]. The results are used to assess the overall quality of original seismic field records (Park, 2015).

Figure 9 displays the SN ratio (%) across approximately 95 individual records along the Tr-7 traverse. The overall SN value is 62%, corresponding to the "good" quality category. Most records fall within the fair (40–60%) and good (60–80%) ranges, indicating generally reliable data quality. A single outlier (record ~26) exhibits a markedly reduced SN ratio (<10%), falling within the unusable range. The color-coded classification (excellent, good, fair, poor, unusable) provides a visual assessment of data reliability.

Subsequently, dispersion curves were generated for all recorded data in each traverse, with frequency band used is 20-50 Hz, minimum depth is 0, whereas maximum depth is 25 m, damping factor value range between 0.1 to 0.3, smoothing factor is 0.4 and lower misfit value, as shown in Fig. 10. At the beginning of the image a somewhat complicated pattern with one strong energy trends appears to be aligned along a constant phase velocity of 1000 m/sec for record (shot) 9 and 1500 m/sec for record (shot) 34 in Tr-7 traverse. Subsequently, dispersion curves were generated for all recorded data in each traverse.

The shear wave velocity for all traverses of the first layer varied from 339 to 401 m/s, for the second layer 507 to 949 m/s and for the third layer 1159 to 1525 m/s. Except for the MS-Tr-7 traverse, the shear wave velocity for the first layer was 929 m/s because the soil thickness of the first layer is thin and mixed with gravel from rock fragments of the second layer due to weathering and calculated alongside the second layer. This traverse was conducted from the outcrop of the Kometan Formation and the range of shear wave velocity results for the first

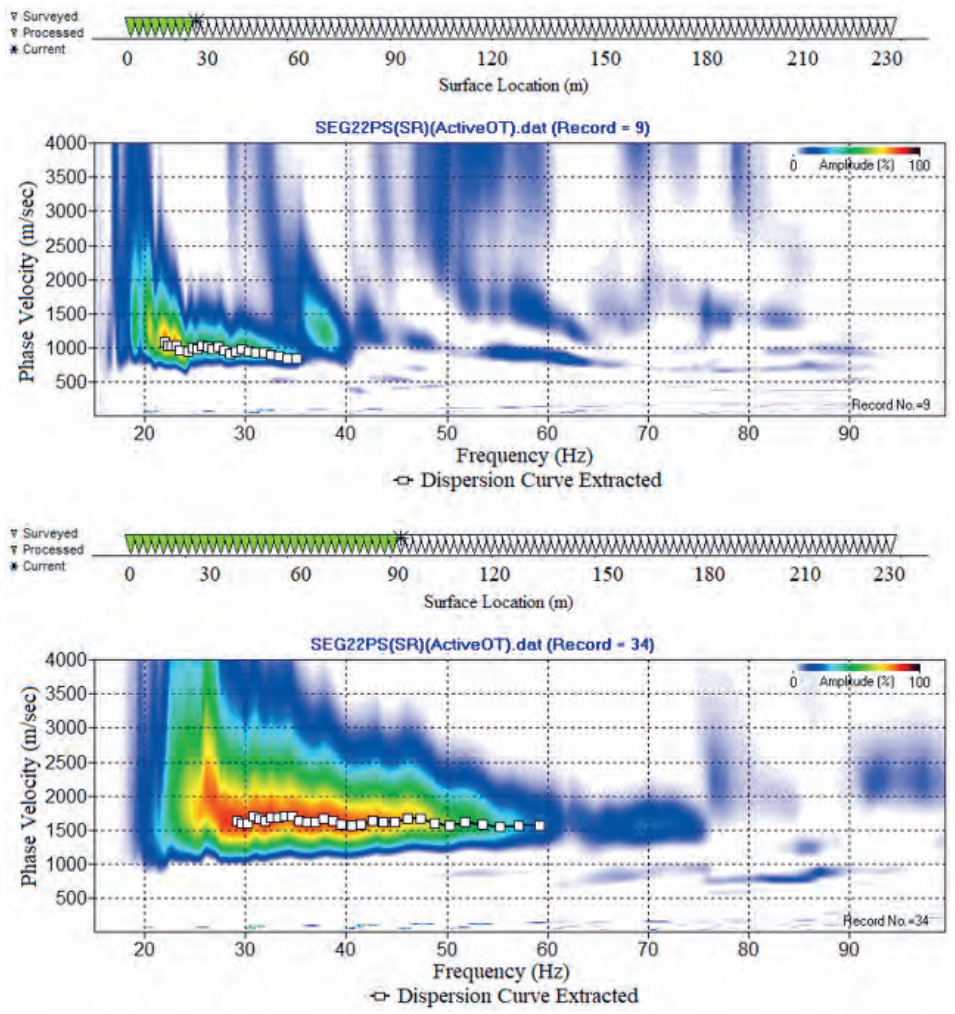


Figure 10. Extracted dispersion curve for record (shot) 9 and 34 in Tr-7 traverse.

and second layers is approximately similar. The MASW resolution limit for thin layers depends on the vertical resolution and wavelength (λ) of the surface wave. Increasing the frequency of the source used in the field decreases the wavelength and improves the resolution of thin layers. A short inter-receiver spacing in this study (2m) applied that is essential to generate the high-frequency and short-wavelength waves that are necessary for good vertical resolution.

The 2D shear wave velocity sections obtained from all MASW traverses depend on V_S values and consist of three lithological layers: surface soil on top, rock fragments in the middle, and limestone at the bottom. The interface between

Table 3. Site classification based on shear-velocity (V_S) ranges (NEHRP soil type) (BSSC, 2003).

Site Class	S-Velocity (*Vs*) (m/sec)
A (Hard Rock)	> 1500
B (Rock)	760–1500
C (Very Dense Soil and Soft Rock)	360–760
D (Stiff Soil)	180–360
E (Soft Clay Soil)	< 180

the first and second layers is invisible because the first layer is thin, while the interface between the overburden layer (first and second layer) and the third layer is clearly visible. The third layer was found to be in good agreement with average shear wave velocities (V_S) of the competent limestone (Kometan Formation), which clearly coincides with the National Earthquake Hazard Reduction Program (NEHRP) Classification (BSSC, 2003). According to this program reliability, the Materials having $V_S > 760$ m/s are considered as rocks and hard rocks, which are located within B (Hard rock) range (Table 3).

Large scale dam study was conducted by Hamed el al. (2024) using the 1D MASW technique to estimate the velocities of the shear wave for the upper 30m (V_{S30}) to provide the site classes and soil characteristics along both sides of the detected Spillway Fault trace in the study area. The calculated V_{S30} values emphasized the idea of the existence of a normal dip-slip fault trace which divides the study area into two different lithological parts. The first part is located on the eastern side and characterized by almost class B (hard rock, according to NEHRP classification), while the other part is located to the west, and shows almost class type C (denoted as dense soil and soft rock soil).

4.3.1. MS-Tr-1 traverse

One-dimensional shear wave velocity was generated for the MS-Tr-1 traverse, and it trends from southwest (SW) to northeast (NE), as shown in Fig. 11. According to this traverse, in the first and second layers, the presence of water in recent deposits depends on the V_S value.

The shear wave velocity (V_S) data obtained across all traverses demonstrated excellent agreement with previous geophysical investigation, Seismic Refraction Tomography (Baban et al., 2022) and joint Electrical Resistivity Tomography / Induced polarization surveys. The V_S findings were also consistent with documented lithology of the one borehole and two water wells near the study area. The interface between the first layer (soil) and the second layer (rock fragments) is not clearly visible in the 2D MASW traverse because the first layer is thin, while the interface between the overburden (first and second layer) and the third layer is obvious (Fig. 12). The average shear wave velocity (V_S) for the first layer

is 391 m/s, indicating soil, and 538 m/s for the second layer, indicating rock fragments, according to the National Earthquake Hazard Reduction Program (NEHRP) soil classification. The overburden layer consists of the first and second layers (top light blue to green line) and has a thickness of 7–14 m.

The high average V_S values of 1159 m/s can be classified as unit B, which is considered as rock (limestone), at a depth of more than 7 m from the right-hand side, 14 m from the central part, and 13 m from the left-hand side (below the light blue to green line). The topography of the third layer is irregular due to weathering. From distances 0–18 m, 23–56 m, and 70–120 m, three collapses were observed, and another collapse is visible at a distance of 134–182 m. Three uplifts were observed at distances 17–34 m, 53–81 m, and 103–134 m. One void is present at depths 17–30 m and at a distance of 97–109 m. The variation in color in the third layer represents fractured limestone, except for the black color, which represents solid and compact limestone that is obvious below a depth of 16 m depending on the previous works. Seismic Refraction Tomography (Baban et al., 2022) and joint Electrical Resistivity Tomography/Induced Polarization surveys. The V_S findings were also consistent with the documented lithology of the one borehole and two water wells near the study area.

This traverse shows that the area consists of three geological layers; the first layer is generally regular and flat, consisting of soil, having a thickness of (0.96–2.45 m). The second layer generally has many lateral variations on the top of the layer, and consists of rock fragments with a thickness ranging between 6.47–11.20 m. This velocity shows that the overburden layers consist of unconsolidated material for first and second layers, which are saturated recent (alluvial) deposits (clay, sand, gravel, and fragments of limestone).

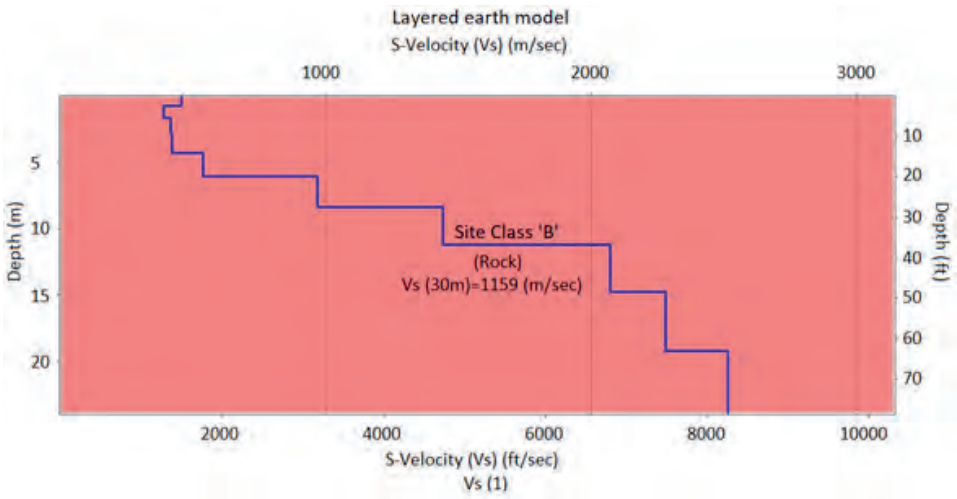


Figure 11. One-dimensional shear wave velocity for MS-Tr-1 traverse.

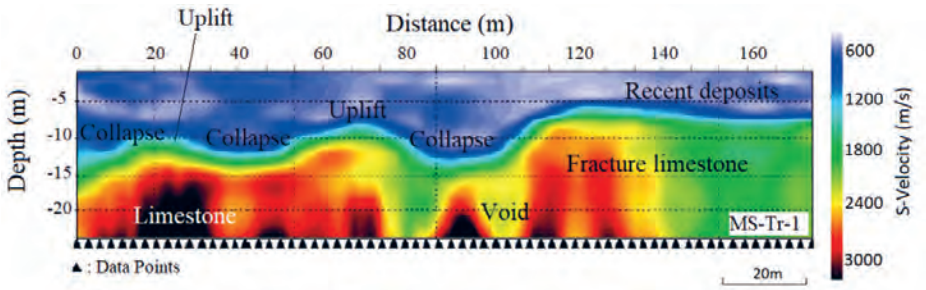


Figure 12. Two-dimensional shear wave velocity for MS-Tr-1 traverse.

The third layer generally has irregular surface and consists of fractured limestone (Kometan Formation) in a depth ranging between 7.4 and 13.7m. The bedrock varies in depth from SW to NE. The results show weathered limestone at depth ranges from 6.47 to 30m, the shallowest depth in the SW part and it is deep in the NE part.

4.3.2. MS-Tr-4 traverse

The MS-Tr-4 traverse trends from southwest (SW) to northeast (NE) and it was analyzed for one-dimensional velocity (V_S), as shown in Fig. 13. Soil stiffness generally decreases when water is present in a layer, as saturation softens the soil matrix and reduces the shear wave velocity and V_S. Velocity increases with depth. This traverse reveals that the average V_S for the first layer is 413 m/s, indicating soil and having a thickness of 0–3.4 m. The second layer generally

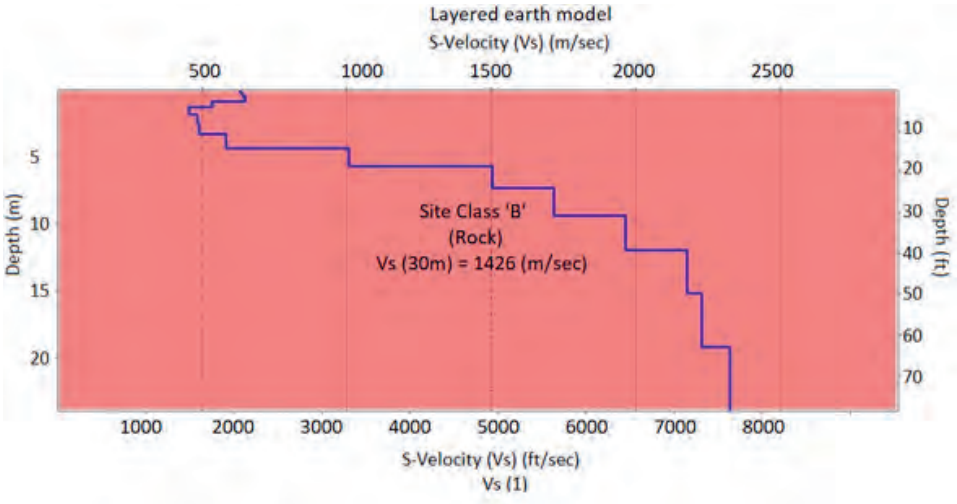


Figure 13. One-dimensional shear wave velocity for MS-Tr-4 traverse.

shows many lateral variations at the top, with a thickness ranging between 3.5 and 12.5 m. It consists of rock fragments and has an average V_S of 534 m/s, which exceeds that of the first layer. This velocity shows that the overburden layers consist of unconsolidated material for first and second layers, which are saturated recent (alluvial) deposits (clay, sand, gravel, and fragments of limestone).

Additionally, the third layer exhibits an average V_S of 1426 m/s and can be classified as unit B, corresponding to rock material according to the NEHRP soil classification. According to Abdelrahman (2025), V_S in weathered limestone varied from 1500m/s to 3500ms. The bedrock varies in depth from SW to NE. The results show weathered limestone at depth ranges from 3.5 to 30 m, the shallowest depth in the center, while it is deep in the SW and NE part.

The topography of the Kometan limestone, as it appears in these traverses, is irregular due to weathering, fracturing, erosion and compacted layer as a result of tectonic movement and stress in the area, which have generated collapse or void and filled with sediments of recent deposits.

The 2D shear wave velocity section is depicted in Fig.14. Within the top 4 to 13 m (indicated by the top light blue to green color line), both the first and second layers are present, representing recent deposits. Their interfaces remain invisible due to the thinness of the first layer. However, collapses that were subsequently filled with sediments have resulted in some areas having thicker recent deposits.

Beneath the light blue to green line, a third layer becomes apparent. The interface between this third layer and the overburden composed of recent deposits from the first and second layers is easily recognizable. Lateral variations are numerous, leading to several collapses filled with recent deposits. Specifically, there are four small collapses at distances of 10–40 m, 45–70 m, 85–117 m, and 130–170 m. Between distances 180–215 m, numerous small voids are represented by yellow spheres and elliptical shapes. Notably, one of these voids occurs at a distance of 205–215 m and extends to a depth of 10–15 m. Additionally, a

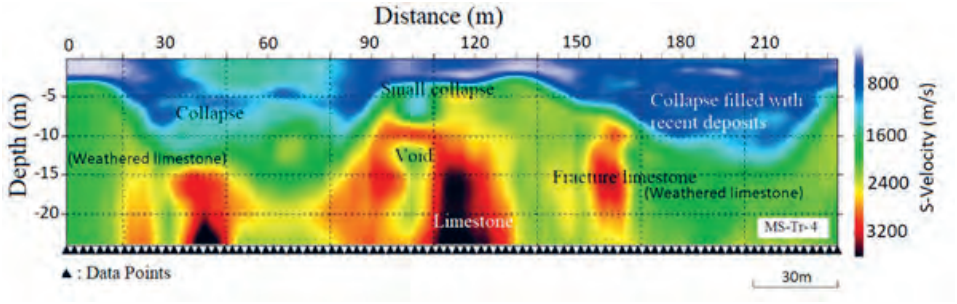


Figure 14. Two-dimensional shear wave velocity for MS-Tr-4 traverse.

layer of weathering is evident below the interface, characterized by variable colors (except black) based on variations in V_S value and fractures.

Finally, solid and compact limestone appears at a distance of 40–50 m and 105–127 m, represented by the color black below a depth of 16 m and an average V_S is 1426 m/s.

4.3.3. MS-Tr-6 traverse

The obtained 1D shear-wave velocity is shown in Fig. 15, trending from southwest (SW) to northeast (NE). This traverse reveals that the average V_S for the first layer is 362 m/s, signifying soil. The average V_S for the second layer is 629 m/s, composed of rock fragments and having a greater velocity than the first layer. Additionally, the average V_S for the third layer is 1353 m/s, classified as unit B, which corresponds to rock material according to the NEHRP soil classification.

The first and second layers consist of recent deposits, and the presence of water in these deposits can be determined based on the variation in shear velocity. Increasing water saturation typically leads to a decrease in V_S. This relationship occurs because higher water content reduces soil stiffness, which directly lowers the shear modulus and the shear wave velocity. MASW detected this stiffness by measuring the resulting V_S, velocity increase with depth, an average V_S of 431 m/s for first layer, the second layer having an average V_S of 534 m/s and the third layer exhibits an average V_S of 1426 m/s. The previous studies, when compared with this study, resulted in a significant correction (Baban et al., 2022).

By combining several 1D shear velocities, a 2D shear velocity is generated. The 2D MASW for the MS-Tr-6 traverse is shown in Fig. 16. The velocity section of the depth investigation comprises three lithological layers. Although it is impossible to clearly identify the interface between the first and second layers due to the thinness of the first layer, they are present from the top 4 to 10 m (indicated by the top light blue to green color line). Some areas have thicker recent deposits than this level due to collapses filled with sediments from recent deposits.

The third layer and the overburden layer are distinctly separated by the interface (light blue to green color line). Below this interface, a third layer becomes evident. Numerous depressions occur at distances of 0–42 m, 45–73 m, 87–105 m, 110–150 m, and 150–230 m. Additionally, a void exists between depths of 16–25 m at a distance of 67–91 m. At the top of the third layer, an elongated collapse shape in green to yellow color is visible at a depth of 10–28 m between distances 107–145 m. The color below the interface in the upper part of the third layer varies due to changes in V_S value, indicating weathering and fractures. Finally, the black color represents compact and solid limestone (Kometan Formation). The result shows MASW can detect both laterally and vertically change

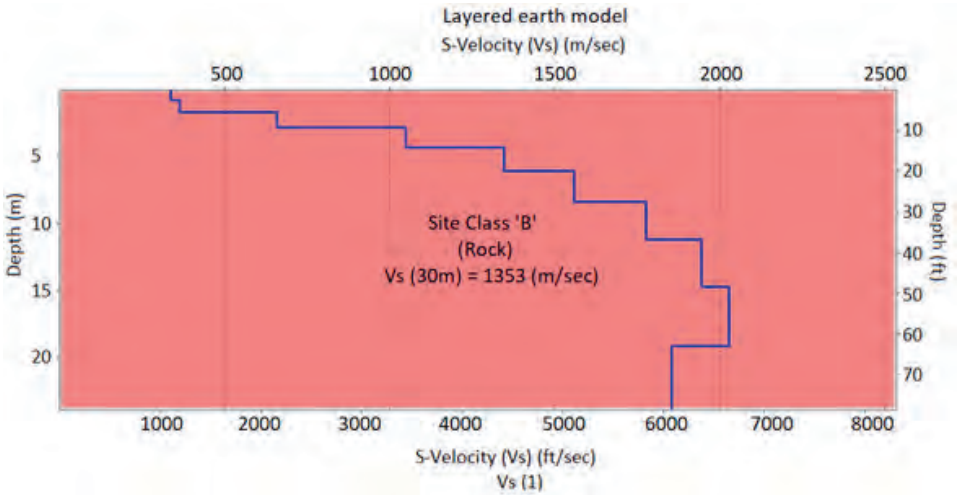


Figure 15. One-dimensional shear wave velocity for MS-Tr-6 traverse.

and can detect void. The bedrock varies in depth from SW to NE. The results show weathered limestone at depth ranges from 5.0 to 30 m, the deepest depth in the beginning SW part.

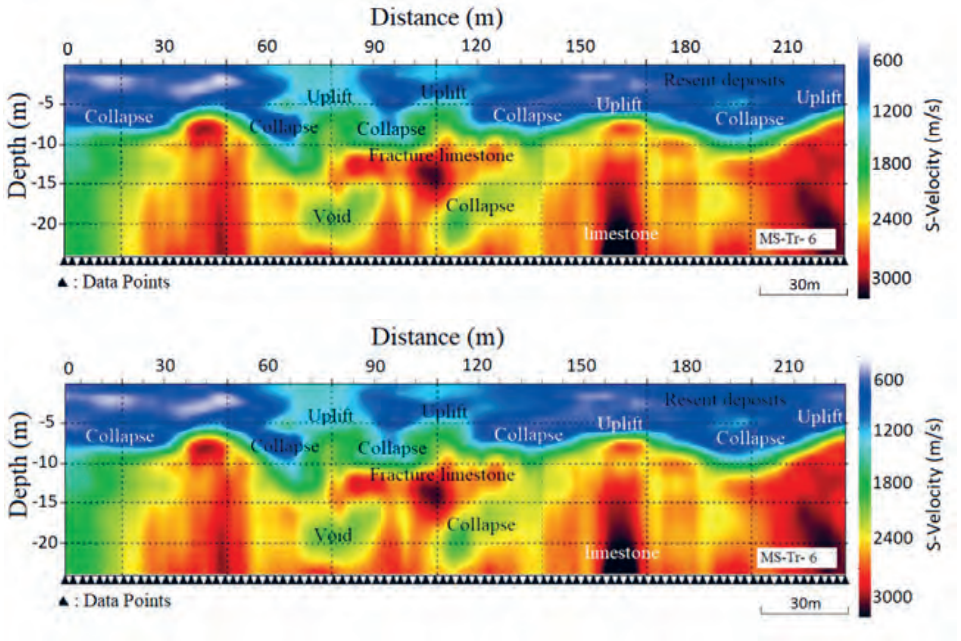


Figure 16. Two-dimensional shear wave velocity for MS-Tr-6 traverse.

The first layer is mainly regular and flat, consists of soil, having a thickness of 1.05–1.97 m. Many lateral variations are present on top of the second layer and consist of rock fragments with a thickness ranging between 7.13 and 10.24 m. The third layer has an irregular surface and consists of fractured limestone of the Kometan Formation, lying at depths ranging from 8.2–12.2 m.

ParkSEIS software can efficiently map subsurface structures using the MASW method, and a 2D V_S traverse is essential for determining the extent and shape of voids and collapses by showing the low-velocity zones that correspond to them. In a 2D V_S traverse the void and collapse shapes are clearly observed. In the study area, collapses are generated by weathering, whereas voids are formed as a result of collapse.

4.3.4. MS-Tr-7 traverse

One-dimensional shear wave velocity was generated for the MS-Tr-7 traverse, trending from southwest (SW) to northeast (NE). Figure 17 illustrates the resulting 1D shear-wave velocity profile. A 1D (depth) profile is obtained by importing a single dispersion-curve file (*.DC), whereas a 2D V_S cross-section (depth and surface distance) is produced by importing multiple dispersion-curve files. Each dispersion curve is analyzed or inverted to obtain a 1-D V_S profile, in which the "theoretical" (or "modeled") fundamental-mode (M0) dispersion curve fits the input "measured" curve most closely using a generic searching algorithm (Park, 2015).

The MS-Tr-7 traverse reveals that the thickness of the first and second layers, composed of recent deposits, varies from 4 to 11 m. Notably, this thickness changes and becomes thicker in collapse areas. The bedrock varies in depth from SW to NE. The results show weathered limestone at depth ranges from 4.0 to 30 m, the deepest part in the beginning of the SW part.

Specifically, the average V_S for the first layer is 929 m/s, suggesting soil mixed with rock fragments (weathered layer consists of soil, sand and gravel). The first and second layer of the study area consists of recent deposits, recent deposits composed of soil and rock fragments, while the average V_S for the second layer is 949 m/s, indicating rock fragments and surpassing the velocity of the first layer. The interface between first layer (soil) and second layer (rock fragments) is not clearly visible in the 2D MASW traverse because the first layer is thin and mixed with rock fragments while interface between overburden (first and second layer) and third layer obvious. According to the NEHRP soil classification, the average V_S for the third layer is 1525 m/s, categorizing it as unit B, a hard rock.

The recently deposited materials primarily consist of the first and second layers. The presence of water in these recent deposits becomes evident through the variation in shear velocity. By comparing this result with the previous work (SRT and ERT method) provided good correlation with one borehole and two wells near the study areas. According to Baban et al. (2022), the result shows

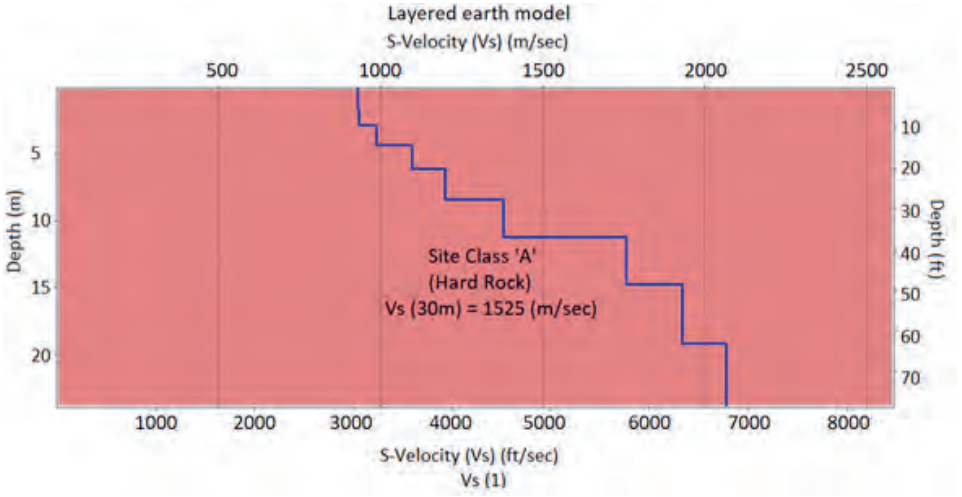


Figure 17. One-dimensional shear wave velocity for MS-Tr-7 traverse.

the presence of shallow ground water in recent deposits at the depth ranges between 2.0–14 m and on the basis of the resistivity values indicates the presence of ground water in the fracture of Kometan limestone.

Figure 18 illustrates the 2D MASW for the MS-Tr-7 traverse. In this section, the interface between the cover soil layer and the rock fragments in the second layer is not clearly visible due to the thinness of the first layer (soil). However,

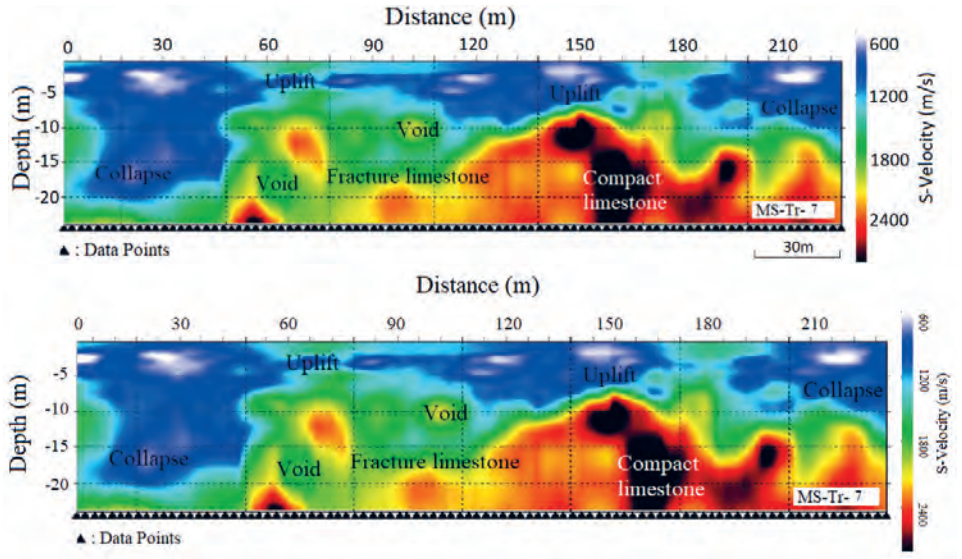


Figure 18. Two-dimensional shear wave velocity for MS-Tr-7 traverse.

the interface between the overburden layer (composed of the first and second layers) and the third layer is distinctly visible.

A significant collapse is observed from the beginning of the traverse up to a length of 60 m, with depths ranging between 4–23 m and filled with recent deposits. Additionally, there are three depressions at distances of 79–150 m, 150–165 m, and 175–230 m. The survey identified two distinct light green color anomalies along the traverse, located at distances from 55 to 120 meters and from 167 to 190 meters, respectively. These anomalies extend to shallow depths, ranging from 0 to 3.7 meters. This specific coloration is interpreted as evidence of fractured limestone. It is noteworthy that the measurements along this traverse were initiated from the exposed outcrops of the Kometan Formation. Furthermore, a light green sphere-shaped area is observed at distances between 189–199 m, with depths of 6.5–8 m. This area consists of fractured limestone pieces resulting from erosion. Finally, the black color represents compact and solid limestone, visible at a depth of 11 m.

The first (soil) layer is regular and flat, having a thickness of 0.05–2.36 m. The top of the second layer generally has many lateral fluctuations and consist of rock fragments with a thickness ranging between 1.93–9.89 m. The surface of the third layer is irregular and consist of fracture limestone (Kometan Formation) in a depth ranging from 2.0–12.3 m.

4.4. Interpretation of the calculated dynamic moduli of elasticity results

The MASW method is applied to solve engineering problems by calculating dynamic moduli of elasticity. According to the MASW velocity results, many engineering dynamic moduli can be determined, which are extremely beneficial for construction purposes. Discovering subsurface dynamic moduli of elasticity typically requires direct measurements with high resolution, providing local information. However, this approach can be costly and time-consuming, often yielding only partial results.

In the present study, the calculations of V_P and V_S will lead to the determination of several key parameters using dynamic elasticity parameters and equations (as shown in Table 4). By analyzing the data, determining velocities, and substituting relevant equations for the first, second, and third layers, the following results were obtained.

The uppermost layer exhibits rock quality ranging from incompetent to fairly competent, with Poisson's ratio between 0.35 and 0.39. The elastic modulus varies from 5.49 $N/m^2 \times 10^8$ to 48.16 $N/m^2 \times 10^8$, the shear modulus ranges from 2.01 $N/m^2 \times 10^8$ to 17.45 $N/m^2 \times 10^8$, and the bulk modulus spans from 9.49 $N/m^2 \times 10^8$ to 90.02 $N/m^2 \times 10^8$. The inverse values of the bulk modulus yield compressibility ranging from 0.10 to 0.01 $m^2/N \times 10^{-8}$. These elasticity moduli suggest that this layer consists of unconsolidated recent sediments affected by weathering processes due to seasonal rainfall. Traverses beyond the 11th reveal

the presence of a stream formed by water flow through the collapsed part of the constructed dam, resulting in the removal of recent sediments and the exposure of bedrock covered by clastic debris, leading to moderate elasticity values.

The second layer's elasticity moduli indicate fairly to moderately competent rock quality, with Poisson's ratio ranging from 0.30 to 0.33. The elastic modulus varies from 12.31×10^8 to 45.58×10^8 N/m², the shear modulus ranges from 4.63×10^8 to 17.59×10^8 N/m², and the bulk modulus spans from 16.99×10^8 to 60.69×10^8 N/m². Compressibility falls within the range of 0.05 to 0.01×10^{-8} m²/N.

The third layer, characterized by good competent rock quality, exhibits Poisson's ratio between 0.24 and 0.25. The elastic modulus varies from 55.31×10^8 to 121.93×10^8 N/m², the shear modulus ranges from 22.21×10^8 to 49.29×10^8 N/m², and the bulk modulus spans from 65.76×10^8 to 142.94×10^8 N/m². Compressibility falls within the range of 0.01 to 0.06×10^{-8} m²/N.

From the analysis of data, velocities and densities were determined and then substituted into the relevant equations for calculating geotechnical engineering parameters (dynamic moduli of elasticity) for the first, second, and third layers, as shown in Table 5.

Based on these results, the Poisson's ratio ranges between 0.35 and 0.39 for the first layer, which characterizes it as having a relatively high Poisson's ratio. This suggests incompetence to fairly competent soil. In the second layer, the Poisson's ratio falls between 0.30 and 0.33, indicating fairly to moderately competent soil or rock. In contrast, the third layer exhibits a Poisson's ratio ranging from 0.24 to 0.25, characterizing it as relatively low and suggesting good competence in rock material (Table 6).

Table 4. Dynamic moduli of elasticity equations from the average shear wave velocity analysis of MASW technique calculated

Rock parameters	Equation	Reference	Remarks
Poisson's Ratio (σ)	$\sigma = \frac{V_P^2 - 2V_S^2}{2(V_P^2 - V_S^2)}$	Andrea et al., (1965) Potter and Fottinek (1997)	V_P = compressional waves velocity V_S = shear waves velocity ρ = bulk density of the material, Vo = reference unit weight values Vo = 17 for dense sand and gravel, and Vo = 18 for limestone
Young's modulus (E)	$E = 2\rho V_S^2(1+\sigma)$		
Shear modulus (μ)	$\mu = \rho V_S^2$		
Bulk modulus (B)	$B = \rho V_P^2 - \frac{4}{3}\mu$		
Compressibility (K)	$K = \frac{1}{B}$		
General density	ρ = Vo + 0.002 * V_P	Tezcan et al. (2006)	

Table 5. Dynamic Moduli of elasticity from the average shear wave velocity analysis MASW technique.

Layers	P-Velocity	S-Velocity	Poisson's Ratio	Density	Young's modulus	Shear modulus	Bulk modulus
	V_P m/sec	V_S m/sec	σ	ρ kg/m^3	E N/m$^2 \times 10^8$	μ N/m$^2 \times 10^8$	B N/m$^2 \times 10^8$
First Layer	737	339	0.35	1747	5.49	2.01	9.49
	2110	929	0.39	2022	48.16	17.45	90.02
Second Layer	973	507	0.30	1795	12.31	4.63	16.99
	1763	949	0.33	1953	45.58	17.59	60.69
Third Layer	2005	1159	0.24	1966	55.31	22.21	65.76
	2597	1525	0.25	2119	121.93	49.29	142.94

Table 6. Classification of soil's competent according to Poisson's ratio (Khalil and Hanafy, 2008)

Soil description	Incompetent to slightly competent	Fairly to moderately competent	Competent material	Very high competent materials
Poisson's Ratio (σ)	0.41–0.49	0.35–0.27	0.25–16	0.03–0.12

5. Discussion

In this research, the MASW method was applied to determine the shear wave velocity (V_S) value. The results revealed the presence of three geologic strata in the area: a surface soil layer on top, rock fragments in the middle, and limestone at the bottom. The shear wave velocities for all traverses varied from 339 to 401 m/s for the first layer, 507 to 949 m/s for the second layer, and 1159 to 1525 m/s for the third layer. However, the MS-Tr-7 traverse had a shear wave velocity of 929 m/s for the first layer because rock fragments mixed with soil and this traverse survey. This difference can be attributed to the thinness of the first layer, which was calculated together with the second layer. Moreover, this traverse was conducted from an outcrop of the Kometan Formation, where the shear wave velocity results for the first and second layers were approximately similar.

The first layer is not clearly visible in the 2D shear wave velocity tomography, and the interface between the first and second layers is invisible. Consequently, the MASW method used in this research was unable to separate the first layer from the second layer due to the thinness of the first layer. However, the method was able to distinguish the overburden layer (recent deposits composed of soil and rock fragments) from the third layer.

Additionally, it can differentiate between weathered and fractured rock and hard bedrock based on variations in V_S. The length of the traverse delineates the depth of penetration by the MASW technique, in which the distance between geophones was minimized to 2 m for the purpose of identifying lateral lithologi-

cal variations within the penetrated layers using seismic refraction waves (V_P and V_S). The stiffness of the bedrock showed significant variation, likely due to various levels of weathering and fracture. The thickness of the overburden (first and second layers) approximately ranges from 7 to 14 m. Below this range, fractured limestone is visible, and the black colour indicates hard and compact limestone. This method is useful for recognizing collapses and voids.

The three-dimensional image in Fig. 19 shows that the study area is topographically flat, with an overall elevation difference of approximately 5 meters. The lowest elevation is located in the southwestern part, near the Chaq-Chaq Dam where the Chaq-Chaq stream passes. In contrast, the highest areas are situated in the eastern part. Due to high average precipitation and a westward upstream water flow, the area experiences uncontrolled water runoff, particularly in the lower-lying southwestern section. This leads to water stress accumulating at the wall of the dam in this part. This is one reason resulting in the failure of the dam wall in that region. Failure of dams can result from internal and external factors. Studies show that dam failure events appear as a result of different reasons such as piping, overtopping, and settlement (Dinçergök, 2007).

MacDonald and Langridge-Monopolis (1984) analyzed 42 events. Their study sample comprised an earthfill with a clay core, and rockfill dams. They estab-

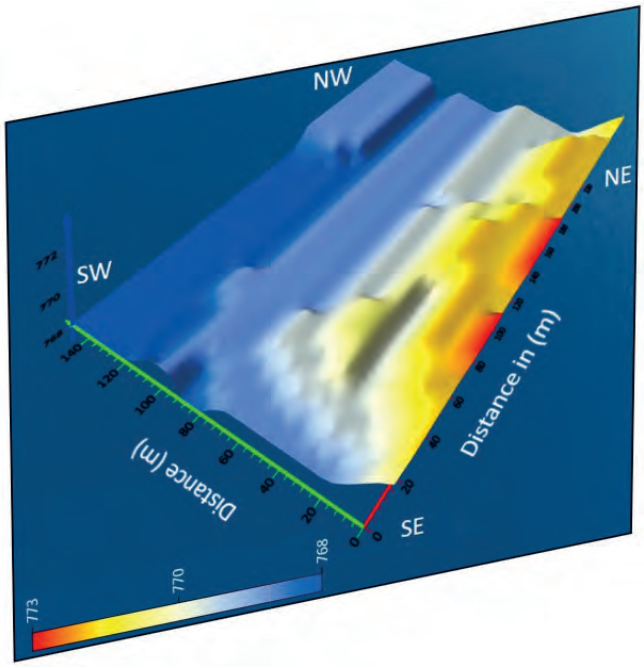


Figure 19. Surface map of the study area.

lished a relationship for the Breach Formation Factor. The factor was estimated by the volume of water that leaves the dam and the depth of water above the dam. Thereafter, the factor was utilized to correlate the amount of the material that was eroded from the dam.

The maximum depth for investigation is approximately 30 m. This method has limited investigation depth and is widely applied for shallow investigations, such as engineering assessments. It is suitable for recognizing shallow subsurface features, including collapses, voids, and detected bedrock, within this limited depth. Both 1D shear wave velocity traverse and 2D shear wave velocity tomography is generated simultaneously using the MASW method.

The MASW method was applied and provided good correlation with one borehole and two wells near the study areas, as well as outcrops. The characterization of the outcrops supported the results. Three geological layers were determined, and the results were compared with available data from one borehole and two

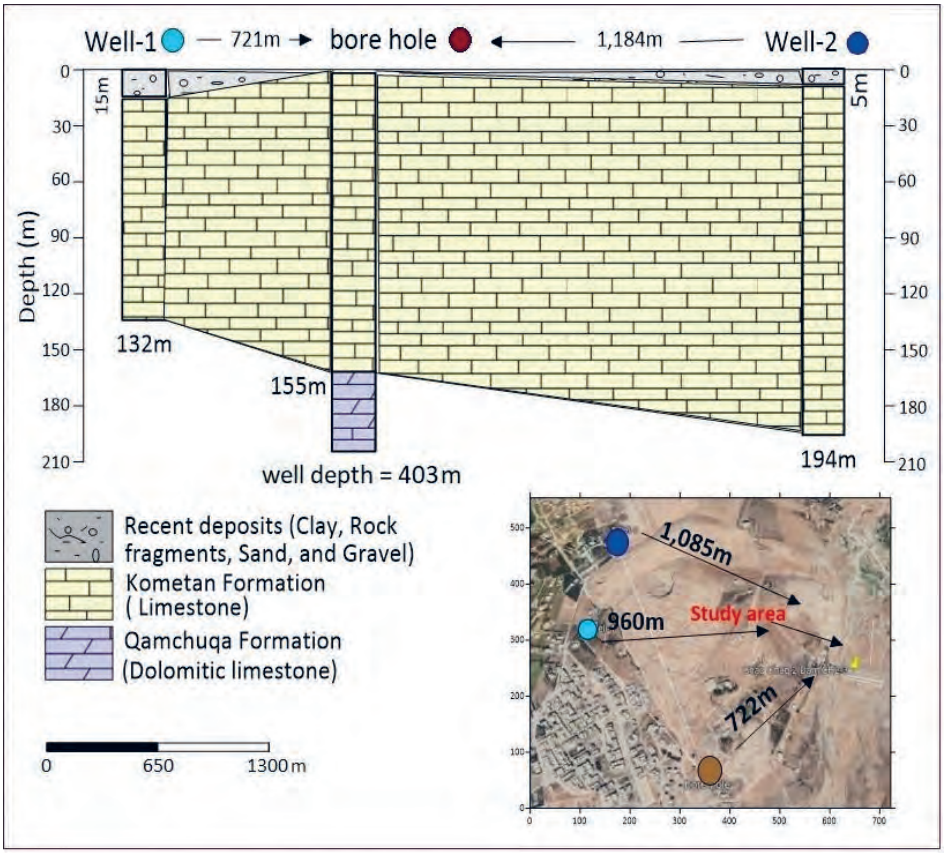


Figure 20. Lithostratigraphic correlation between one borehole and two wells near the study area.

wells near the study area, as shown in Fig. 20. This validation process confirms the reliability of the geophysical data interpretation and its suitability for determining the top of the bedrock.

As a result, several geotechnical parameters were calculated. According to the MASW results, Poisson's ratio ranges between 0.35 and 0.39 for the first layer, between 0.30 and 0.33 for the second layer, and between 0.24 and 0.25 for the third layer. Based on these findings:

- The first layer exhibits a relatively high Poisson's ratio, indicating soil that ranges from incompetent to fairly competent.
- The second layer represents fairly to moderately competent rock.
- The third layer demonstrates a relatively low Poisson's ratio, signifying good competence in the limestone.

The relationship between the compressional wave velocity (V_P) and shear wave velocity (V_S) is linear across the first, second, and third layers, as velocity generally increases with depth. Young's modulus is directly proportional to V_P, while shear modulus is directly related to it. Conversely, Poisson's ratio shows an inverse relationship with the ratios of V_S / V_P for the first and second layers, affecting material brittleness and rigidity. The relationship between V_P for the first and second layers and compressibility is inversely proportional. Additionally, the ratio of bulk modulus (B) to shear modulus (μ) is inversely proportional to the V_S / V_P ratio.

6. Conclusions

The study area comprises three distinct layers: soil, rock fragments, and limestone (Kometan Formation), which align with previous findings (Baban et al., 2022). The first layer exhibits a low shear velocity (V_S), the second layer has a moderate V_S value, and the third layer demonstrates a higher V_S value. Numerous collapses and voids were observed during the investigation. Vs values were determined using the MASW method, allowing for the calculation of various geotechnical parameters. Additionally, this method can predict water content in recent deposits based on variations in V_S values.

The interface between the first and second layers remains invisible in the V_S section due to the thinness of the first layer. However, it can differentiate between weathered bedrock and hard bedrock based on V_S variations. The stiffness of the bedrock exhibits significant variability, likely attributed to different levels of weathering. The overburden thickness (comprising the first and second layers) ranges approximately from 7 to 14 meters. Below this depth, fractured limestone becomes visible, followed by hard limestone. The maximum investigation depth is approximately 30 meters. Both 1D shear wave velocity traverses and 2D shear wave velocity tomography is generated simultaneously using the MASW method, the geotechnical parameters estimated from equations are tak-

ing into account the required data represented in these equations like (density, depths), as well as layers boundary and their lithology from two boreholes data.

The dam failure resulted from several factors. Firstly, several sinkholes and rock fractures existed at the beginning of most traverses, likely due to water infiltration during the rainy winter season. These sinkholes deepened over time, contributing to the dam's failure. Notably, the sinkhole in the western part played a significant role in the dam's collapse under water pressure.

In addition, the dam's basic design lacked scientific rigor, and uncontrolled water flow occurred due to maximum average precipitation. Water flowed upstream toward the western part of the area, specifically the southwestern region, exerting stress on the dam wall and leading to its collapse. Other contributing factors included inadequate compaction during dam construction and the use of rock fragments without concrete in the spillway. Moving forward, climate considerations, especially maximum average precipitation, should be integral to dam design to prevent uncontrolled water flow. The above results are supported by seismic refraction tomography (SRT), electrical resistivity tomography (ERT) and multichannel analysis of surface waves (MASW) conducted by Hamed el al. (2024). According to the seismic refraction profiles, they noticed that the detected fault caused relatively considerable displacement in the sedimentary and basement rocks.

In this study, the presence of a borehole is important for comparing geophysical layer thicknesses with those obtained from the borehole. Using seismic method, both V_P and V_S velocities were determined. We applied these velocities to estimated geotechnical parameters and density, and seismic velocities were used to identify lithology. The MASW method applied in this study plays a crucial role and is an effective method for detecting collapses and voids that cause failure in the region, as observed in Figs. 12, 14, 16 and 18.

7. Recommendations

- The results are crucial for redesigning the collapsed dam by reconstructing the dam base to a suitable depth within the Kometan Formation, at least 15-39 m deep using concrete. Additionally, the dam design should incorporate three automatic gates along the main spillway to regulate water release into the Qliasan stream during the summer season. The dam's shoulder should be securely intertied with the adjacent rock, extending at least 5 meters on both sides of the dam.
- The failed section of the dam can be remedied through a grounding process, ensuring it is securely tied to the remaining intact part of the dam.
- The dam must withstand the hydrostatic pressure exerted by the reservoir water when filled. This design consideration ensures the dam's safety, especially during unexpected natural events like flooding. The spillway

and gates will effectively manage flood effects, maintaining controlled water levels in the lake and the Qliasan stream throughout all seasons.

- In the future, 3D (SRT or ERT) methods are preferable for achieving accurate and high subsurface resolution. These techniques can detect bedrock and other features effectively.

Acknowledgments and data availability – The authors would like to express their sincere gratitude to the Governorate of Sulaimani, Kurdistan Region, Iraq, for their continuous support and for providing the facilities necessary to conduct this research. We also extend our appreciation to the Department of Social Sciences, College of Basic Education, University of Sulaimani, for their valuable academic guidance and constructive feedback throughout the study. Special thanks are due to the Department of Geology, College of Science, University of Sulaimani, for their technical assistance, scientific input, and access to laboratory resources that significantly contributed to the completion of this work. The raw data supporting the conclusions of this article will be made available by the authors upon reasonable request. Basically, all data are presented in the article.

References

Abdelrahman, K. (2025): Shear wave velocity structure at King Saud University, Saudi Arabia, derived from MASW and microtremor arrays, *Sci. Rep.*, 15, 11497, https://doi.org/10.1038/s41598-025-90894-4.

Abudeif, A. M., Fat-Helbary, R. E., Mohammed, M. A., Alkhashab, H. M., and Masoud, M. M. (2019): Geotechnical engineering evaluation of soil utilizing 2D multichannel analysis of surface waves (MASW) technique in New Akhmim City, Sohag, Upper Egypt, *J. Afr. Earth Sci.*, 157, 103512, https://doi.org/10.1016/j.jafrearsci.2019.05.020.

Alavi, M. (2004): Regional stratigraphy of the Zagros fold–thrust belt of Iran and its pro-foreland evolution, *Am. J. Sci.*, 304, 1–20.

Alavi, M. (2007): Structures of the Zagros fold–thrust belt in Iran, *Am. J. Sci.*, 307, 1064–1095, https://doi.org/10.2475/09.2007.02.

Al-Hakari, S. H. S. (2011): *Geometric analysis and structural evolution of NW Sulaimani area, Kurdistan Region, Iraq*, PhD thesis, University of Sulaimani, Iraq, 309 pp.

Al-Qayim, B., Ibrahim, A. O., and Koyi, H. (2012): Tectonostratigraphic overview of the Zagros Suture Zone, Kurdistan Region, northeast Iraq, *GeoArabia*, 17, 109–156, https://doi.org/10.2113/geoarabia1704109.

Arisona, A., Nawawi, M., Khalil, A. E., Nuraddeen, U. K., Hariri, M., and Fathi, M. A. (2017): Evaluation study of boundary and depth of the soil structure for geotechnical site investigation using MASW, *J. Geosci. Eng. Environ. Technol.*, 2, 31–38, https://doi.org/10.24273/jgeet.2017.2.1.21.

Ashraf, M. M., Kumar, N. S., Yusoh, R., Hazreek, Z. A. M., and Aziman, M. (2018): Site classification using multichannel analysis of surface waves (MASW) on soft and hard ground, *J. Phys. Conf. Ser.*, 995, 012108, https://doi.org/10.1088/1742-6596/995/1/012108.

Baban, E. N., Amin, A. K., and Mohammed, S. S. (2022): Seismic refraction tomography and geotechnical parameters to assess the Chaqchaq Dam failure in NW Sulaimani City, Kurdistan Region, Iraq, *Iraqi Nat. J. Earth Sci.*, 22, 121–139, https://doi.org/10.33899/earth.2022.135251.1027.

BSSC (2003): *NEHRP recommended provisions for seismic regulations for new buildings and other structures, Part 1: Provisions*, FEMA 368, Federal Emergency Management Agency, Washington, D.C.

Buday, T. (1980): *The regional geology of Iraq, Vol. 1: Stratigraphy and paleogeography*, Geological Survey of Iraq, Baghdad, 445 pp.

Buday, T., and Jassim, S. (1987): *The regional geology of Iraq: Tectonics, magmatism, and metamorphism*, Geological Survey of Iraq, Baghdad, 445 pp.

Ditmar, V. (1971): *Geological conditions and hydrocarbon prospect of the Republic of Iraq (Northern and Central parts)*, Technoexport report, Baghdad .

Duan, Z., Chen, J., Xie, J., Li, Q., Zhang, H., and Chen, C. (2024): Study on the evolution characteristics of dam failure due to flood overtopping of tailings ponds, *Water*, 16, 2406, https://doi.org/10.3390/w16172406.

Dunnington, H. V. (1958): Generation, migration, accumulation and dissipation of oil in northern Iraq, in: *Habitat of Oil*, AAPG, Tulsa, 1194–1250.

Dinçergök, T. (2007): The role of dam safety in dam-break induced flood management, *Proc. Int. Conf. River Basin Management*, Southampton, UK, 683–691.

Froehlich, D. C. (2008): Embankment dam breach parameters and their uncertainties, *J. Hydraul. Eng.*, 134, 1708–1721, https://doi.org/10.1061/(ASCE)0733-9429(2008)134:12(1708).

Hamed, A., Fat-Helbary, R., Mohamed, A., El-Faragawy, K. O., Abd El-Gaber, A., and Meneisy, A. M. (2024): Application of seismic refraction and MASW methods for investigating the spillway fault trace along the western side of the Aswan High Dam, Egypt, *Acta Geod. Geophys.*, 59, 27–50, https://doi.org/10.1007/s40328-024-00437-y.

ICOLD (1998): *Dam-break flood analysis – Review and recommendations*, Bulletin 111, International Commission on Large Dams, Paris.

Jassim, S. Z., and Goff, J. C. (2006): *Geology of Iraq*, Dolin, Prague, and Moravian Museum, Brno, 341 pp.

Karray, M., Lefebvre, G., Ethier, Y., and Bigras, A. (2010): Assessment of deep compaction of the Péribonka dam foundation using modal analysis of surface waves (MASW), *Can. Geotech. J.*, 47, 312–326, https://doi.org/10.1139/T09-108.

Khalil, M. H., and Hanafy, S. M. (2008): Engineering application of seismic refraction method: a field example at Wadi Wardan, NE Sinai, Egypt, *J. Appl. Geophys.*, 65, 132–141, https://doi.org/10.1016/j.jappgeo.2008.06.003.

Kostecki, S., and Banasiak, R. (2020): The catastrophe of the Niedów dam – the dam break causes, development and consequences, *Nat. Hazards Earth Syst. Sci.*, 20, 1–24, https://doi.org/10.5194/nhess-2020-372.

MacDonald, T., and Langridge-Monopolis, J. (1984): Breaching characteristics of dam failures, *J. Hydraul. Eng.*, 110, 567–586, https://doi.org/10.1061/(ASCE)0733-9429(1984)110:5(567).

Meneisy, A. M., Hamed, A., Khalifa, M., El-Bohoty, M., Ghamry, E., and Taha, A. (2023): Geotechnical zonation and Vs30 classification of soil for seismic site effects evaluation in the western extension of New Aswan City, Egypt, *Pure Appl. Geophys.*, 180, 3813–3833, https://doi.org/10.1007/s00024-023-03370-3.

Netto, L. G., Gandolfo, O. C. B., Filho, W. M., and Dourado, J. C. (2020): Non-destructive investigation on small earth dams using geophysical methods: seismic surface wave multichannel analysis (MASW) and S-wave refraction seismic methods, *Braz. J. Geophys.*, 38, 5–19, http://dx.doi.org/10.22564/rbgf.v38i1.2031.

Park, C. B., and Carnevale, M. (2009): 3D MASW, *Proc. Symp. Appl. Geophys. Eng. Environ. Probl. (SAGEEP)*, Fort Worth, TX, USA.

Park, C. B. (2015). PS User Guide Series: PS – Overview – Description of General Procedure. Kansas Geological Survey, University of Kansas, Lawrence, KS, USA.

Rahnema, H., Mirassi, S., and Dal Moro, G. (2021): Cavity effect on Rayleigh wave dispersion and P-wave refraction, *Earthq. Eng. Eng. Vib.*, 20, 79–88, https://doi.org/10.1007/s11803-021-2006-y.

Taipodia, J., Baglari, D., and Dey, A. (2018): Recommendations for generating dispersion images of optimal resolution from active MASW survey, *Innov. Infrastruct. Solut.*, 3, 1–19, https://doi.org/10.1007/s41062-017-0120-5.

Tsai, C. C., and Lin, C. H. (2022): Review and future perspective of geophysical methods applied in nearshore site characterization, *J. Mar. Sci. Eng.*, 10, 344, https://doi.org/10.3390/jmse10030344.

Wahl, T. L. (1998): *Prediction of embankment dam breach parameters – A literature review and needs assessment*, DSO-98-004, U.S. Bureau of Reclamation, Denver, CO.

Xiong, Y. (2011): A dam break analysis using HEC-RAS, *J. Water Resour. Prot.*, 3, 370–379, http://dx.doi.org/10.4236/jwarp.2011.36047.

Zebari, M., Grützner, C., Navabpour, P., and Ustaszewski, K. (2019). Relative timing of uplift along the Zagros Mountain Front Flexure (Kurdistan Region of Iraq): Constrained by geomorphic indices and landscape evolution modeling. Solid Earth, 10, pp. 663-682, https://doi.org/10.5194/se-10-663-2019.

Zhang, L. M., Xu, Y., and Jia, J. S. (2009): Analysis of earth dam failures: a database approach, *Georisk*, **3**, 184–189, https://doi.org/10.1080/17499510902831759.

SAŽETAK

Procjena geotehničkih parametara primjenom višekanalne analize površinskih valova (MASW) u uzvodnom slivu brane Chaq-Chaq u Sulaimaniji, sjeveroistočni Irak

Sazan S. Mohammed, Abdulla K. Amin and Ezzadin N. Babana

Brzine longitudinalnih i transverzalnih seizmičkih valova (V_P i V_S) određene su na sedam paralelnih profila metodom višekanalne analize površinskih valova (MASW) unutar uzvodnog sliva brane Chaq-Chaq u Sulaimaniji, Kurdistanska regija, Irak. Profili su izvedeni s razmakom od 2 m između geofona. Cilj ovoga istraživanja bio je ispitati geološke značajke, odrediti dubinu do stijenske podloge, procijeniti njenu čvrstoću, izračunati brzine longitudinalnih i transverzalnih seizmičkih valova te istražiti moguće uzroke urušavanja izgrađene brane Chaq-Chaq. Podaci su prikupljani i obrađivani primjenom računalnih programa Geometrics Seismodule Controller i ParkSeis. Rezultati brzina ukazuju na to da se istraživano područje sastoji od tri jedinice različitih geoloških značajki: 1) površinskog sloja tla, 2) srednjeg sloja sastavljenog od stijenskih fragmenata te 3) najdubljeg sloja kojeg čine vapnenci. Izračunati Poissonov koeficijent, temeljen na vrijednostima V_P i V_S za ova tri sloja, iznosi od 0,35 do 0,39 za površinski sloj tla, od 0,30 do 0,33 za tlo sa stijenskim fragmentima te od 0,24 do 0,25 za vapnence. Ovi rezultati upućuju na to da površinsko tlo ima relativno visoke vrijednosti Poissonova koeficijenta, što ukazuje na sloj tla niske posmične čvrstoće, drugi sloj pokazuje umjerene vrijednosti, dok treći sloj ima niske vrijednosti Poissonovog koeficijenta, što upućuje da vapnenci imaju visoku posmičnu čvrstoću. Rezultati također ukazuju na nedostatke u projektiranju brane, osobito u njezinim južnim dijelovima, gdje većina profila pokazuje prisutnost vrtača. Smatra se da su te vrtače uzrokovane procijeđivanjem vode tijekom kišne zimske sezone. Pri djelovanju vodenog tlaka na branu, ove vrtače u jugozapadnom dijelu područja mogu se smatrati jednim od glavnih uzroka urušavanja brane. Dodatno, bočna strana brane nije bila pravilno povezana sa stijenskom masom koja tvori desnu obalu brane.

Ključne riječi: MASW; dinamički moduli; brzina posmičnih valova; brana Chaq-Chaq; Irački Kurdistan

Corresponding author's address: Sazan S. Mohammed, Governorate of Sulaimani, Main Qliasan street, 46001, Sulaimani, Kurdistan Region, Iraq. email: *sazansafa10@gmail.com*

This work is licensed under a Creative Commons Attribution-NonCommercial 4.0 International License.